

The astrophysically important 3^+ state in ^{18}Ne and the $^{17}\text{F}(p, \gamma)^{18}\text{Ne}$ stellar rate

D. W. Bardayan,^{1,2,*} J. C. Blackmon,¹ C. R. Brune,³ A. E. Champagne,³ A. A. Chen,² J. M. Cox,⁴ T. Davinson,⁵
 V. Y. Hansper,^{1,3,†} M. A. Hofstee,⁶ B. A. Johnson,⁴ R. L. Kozub,⁴ Z. Ma,^{1,7,8} P. D. Parker,² D. E. Pierce,¹
 M. T. Rabban,¹ A. C. Shotter,⁵ M. S. Smith,¹ K. B. Swartz,² D. W. Visser,² and P. J. Woods⁵

¹Physics Division, Oak Ridge National Laboratory, Oak Ridge, Tennessee 37831

²A. W. Wright Nuclear Structure Laboratory, Yale University, New Haven, Connecticut 06520-8124

³Department of Physics and Astronomy, University of North Carolina, Chapel Hill, North Carolina 27599

⁴Physics Department, Tennessee Technological University, Cookeville, Tennessee 38505

⁵Department of Physics and Astronomy, University of Edinburgh, Edinburgh EH9 3JZ, United Kingdom

⁶Department of Physics, Colorado School of Mines, Golden, Colorado 80401

⁷Chinese Institute for Atomic Energy, Beijing 102413, People's Republic of China

⁸Joint Institute for Heavy Ion Research, Oak Ridge, Tennessee 37831

(Received 19 June 2000; published 19 October 2000)

Knowledge of the $^{17}\text{F}(p, \gamma)^{18}\text{Ne}$ reaction rate is important for understanding stellar explosions, but it was uncertain because the properties of an expected but previously unobserved 3^+ state in ^{18}Ne were not known. This state would provide a strong s -wave resonance for the $^{17}\text{F}+p$ system and, depending on its excitation energy, could dominate the stellar reaction rate at temperatures above 0.2 GK. We have observed this missing 3^+ state by measuring the $^1\text{H}(^{17}\text{F}, p)^{17}\text{F}$ excitation function with a radioactive ^{17}F beam at the ORNL Holifield Radioactive Ion Beam Facility (HRIBF). We find that the state lies at a center-of-mass energy of $E_x = 599.8 \pm 1.5_{\text{stat}} \pm 2.0_{\text{sys}}$ keV ($E_x = 4523.7 \pm 2.9$ keV) and has a width of $\Gamma = 18 \pm 2_{\text{stat}} \pm 1_{\text{sys}}$ keV. The measured properties of the resonance are only consistent with a $J^\pi = 3^+$ assignment.

PACS number(s): 26.30.+k, 25.40.Cm, 25.60.Bx, 27.20.+n

I. INTRODUCTION

A. Astrophysical importance of the $^{17}\text{F}(p, \gamma)^{18}\text{Ne}$ rate

In extremely hot and dense astrophysical environments such as in novae and x-ray bursts, proton-capture reactions on radioactive nuclei may become faster than their β -decay rates. This occurs because the charged-particle reaction rates increase exponentially with temperature, while the β -decay rates are temperature independent to first-order. The residual elemental abundances produced in these events provide important clues as to the conditions which must have been present during the explosion. Knowledge of the charged-particle reaction rates on proton-rich radioactive nuclei is, therefore, vital for the interpretation of the measured abundances.

Observations (e.g., Ref. [1], and references therein) suggest that novae occur on white dwarves in close binary star systems with extended companion stars that are overflowing their Roche lobes. The dwarf can be either a carbon-oxygen (CO) white dwarf which has formed after the He-burning stage of its evolution, or an oxygen-neon-magnesium (ONeMg) white dwarf which has developed after the carbon-burning stage [2]. Hydrogen-rich material from the companion streams through the inner Lagrangian point, forming an accretion disk before settling onto the surface of the white dwarf. Convection leads to an enrichment of heavier isotopes within this envelope [3]. As the temperature and density

rises, thermonuclear ignition takes place at the bottom of the accreted envelope under degenerate conditions. The temperature rises without a subsequent rise in pressure and a thermonuclear runaway results.

During this runaway, ^{16}O nuclei capture protons to form ^{17}F . The fate of the produced ^{17}F is uncertain and depends on the $^{17}\text{F}(p, \gamma)^{18}\text{Ne}$ rate. If the proton-capture rate is slower than the ^{17}F - β -decay rate at temperatures and densities characteristic of nova explosions ($T \leq 0.4$ GK and $\rho \approx 10^4$ g/cm³), then the reaction sequence $^{17}\text{F}(e^+ \nu_e)^{17}\text{O}(p, \alpha)^{14}\text{N}(p, \gamma)^{15}\text{O}$ occurs. This contributes to the ^{15}O enrichment which is needed to explain the large overabundance of ^{15}N (originating from ^{15}O β decay) observed in nova ejecta [4].

If, on the other hand, the $^{17}\text{F}(p, \gamma)^{18}\text{Ne}$ rate is significant, there can be a substantial flow through the reaction sequence $^{17}\text{F}(p, \gamma)^{18}\text{Ne}(e^+ \nu_e)^{18}\text{F}$, and the $^{18}\text{F}/^{17}\text{F}$ abundance ratio would be altered. Because the temperature in the burning shell rises rapidly, the peak temperature can exceed the Fermi temperature before the electron gas is sufficiently non-degenerate to initiate expansion. This allows a convective zone to develop at the base of the envelope which gradually grows to the surface as the temperature continues to increase. Convection can bring ^{18}F and unburned ^{17}F to the cooler surface regions where they can only β decay. This is important for three reasons. First, the release of the decay energy further increases the luminosity to a level in excess of $10^5 L_\odot$ ($L_\odot =$ solar luminosity $\approx 3.8 \times 10^{26}$ J/s) which can cause rapid expansion and ejection of the envelope [5]. Second, the 511-keV γ rays produced by the annihilation of positrons from the decay of ^{18}F could be detectable. This is possible because the longer half-life of ^{18}F allows it to sur-

*Present address: Department of Physics and Astronomy, University of North Carolina, Chapel Hill, NC 27599.

†Present address: Institute of Physics and Astronomy, University of Aarhus, Ny Munkegade, DK-8000 Aarhus C, Denmark.

vive the expansion phase after which the envelope becomes more transparent [6,7]. Third, the $^{18}\text{O}/^{17}\text{O}$ abundance ratio would be altered which could provide an important constraint on nova models.

Knowledge of the astrophysical $^{17}\text{F}(p,\gamma)^{18}\text{Ne}$ rate is also important for understanding x-ray bursts. The observed spectral features of x-ray bursts suggest interactions involving neutron stars. The standard models are based on accretion in a close binary system onto the surface of a neutron star with an approximate accretion rate of 10^{-10} to $10^{-9} M_{\odot}/\text{year}$ [8]. The accreted matter is continuously compressed by the freshly deposited material until it reaches sufficiently high pressure and temperature to trigger nuclear reactions. The released energy triggers a thermonuclear runaway near the surface of the neutron star under highly degenerate conditions, and peak temperatures up to 2 GK can be reached before the degeneracy is completely lifted.

During the ignition phase of such a burst the temperature rises rapidly, and this triggers proton-capture reactions on the carbon, nitrogen, and oxygen isotopes that have not been destroyed by spallation in the outer atmosphere of the accreting neutron star. Wiescher, Schatz, and Champagne [9] have calculated that during this phase the energy production as a function of time goes through two maxima corresponding to the sudden conversion of ^{12}C into ^{14}O by $^{12}\text{C}(p,\gamma)^{13}\text{N}(p,\gamma)^{14}\text{O}$ and the conversion of ^{16}O into ^{15}O by $^{16}\text{O}(p,\gamma)^{17}\text{F}(p,\gamma)^{18}\text{Ne}(e^+\nu_e)^{18}\text{F}(p,\alpha)^{15}\text{O}$. The second sequence and thus the maximum energy production of the x-ray burst during this phase depend sensitively on the $^{17}\text{F}(p,\gamma)^{18}\text{Ne}$ reaction rate.

The peak of the burst is initiated at a temperature of approximately 0.24 GK via the triple α process. At the same time, the waiting-point nuclei ^{14}O , ^{15}O , and ^{18}Ne , are rapidly depleted by α capture. This leads to the sequence $^{14}\text{O}(\alpha,p)^{17}\text{F}(p,\gamma)^{18}\text{Ne}(\alpha,p)^{21}\text{Na}$ [10] which establishes a continuous flow from helium into the αp -capture process where the energy generation rate can increase by two orders of magnitude [9]. In subsequent rp processing, elements more massive than iron can be synthesized [11]. To understand the conditions under which this flow develops, we need to know the $^{17}\text{F}(p,\gamma)^{18}\text{Ne}$ stellar reaction rate.

B. Previous studies of ^{18}Ne

The $^{17}\text{F}(p,\gamma)^{18}\text{Ne}$ rate is made up of contributions from direct and resonant capture. The direct capture cross section has been calculated in Ref. [12]. Only a few states in ^{18}Ne contribute significantly to the resonant capture rate and, once the properties of those states are known, the resonant capture rate can be calculated. At $T=0.5$ GK, the most effective energy for thermonuclear reactions, $E_0 = 1.22(Z_1^2 Z_2^2 A T_6^2)^{1/3}$ keV [13] where A is the reduced mass in atomic mass units and $T_n = T/(10^9 \text{ K})$, is 326 keV. Therefore, states in ^{18}Ne around $E_x = 4.3$ MeV are the most important for determining the $^{17}\text{F}(p,\gamma)^{18}\text{Ne}$ rate. A nuclear level diagram of ^{18}Ne and its isobars as they were known before the present work is shown in Fig. 1.

Early studies of this excitation energy region in ^{18}Ne were performed using the $^{16}\text{O}(^3\text{He},n)^{18}\text{Ne}$ and

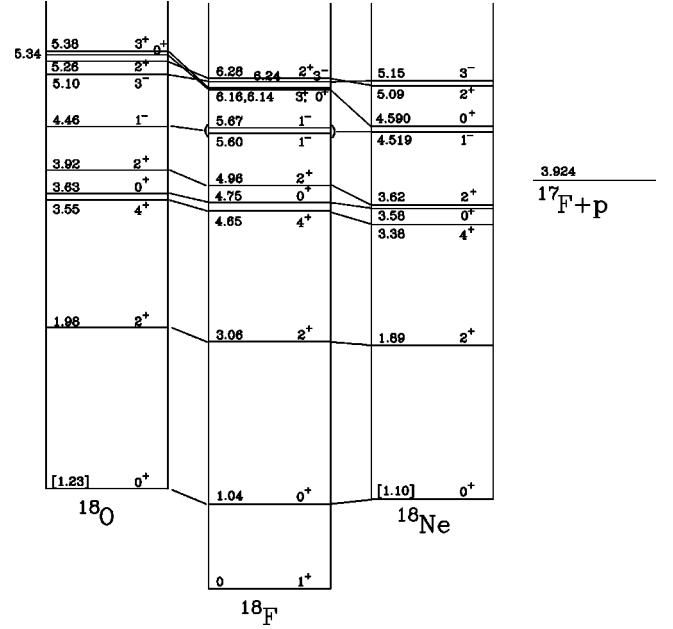


FIG. 1. The nuclear level diagrams for the $A=18$ isobars are shown as they were known before this work. A 3^+ state exists at 5.38 MeV in ^{18}O , but its mirror in ^{18}Ne had never been conclusively observed. This 3^+ state would provide an s -wave resonance and, depending on its excitation energy, could dominate the $^{17}\text{F}(p,\gamma)^{18}\text{Ne}$ rate.

$^{20}\text{Ne}(p,t)^{18}\text{Ne}$ reactions [14–17]. These initial studies, however, were limited by their resolution. Adelberger and McDonald [18] were the first to resolve the states at 4.52 and 4.59 MeV. Nero *et al.* [19] confirmed the excitation energies of these states and assigned the spin and parity as $J^\pi = 1^-$ and 0^+ for the 4.52 and 4.59 MeV states, respectively. Nero *et al.* were also the first to resolve the states at 5.09 and 5.15 MeV. They assigned $J^\pi = 2^+, 3^-$ to the 5.1 MeV doublet, but they could not identify which state had which spin. There was no evidence for any other states in this energy region.

Wiescher, Görres, and Thielemann [20] predicted that the mirror to the 3^+ state at $E_x = 5.38$ MeV in ^{18}O should have an excitation energy of $E_x = 4.328$ MeV in ^{18}Ne and a width $\Gamma \approx \Gamma_p = 5$ keV. This low-energy 3^+ state could dominate the $^{17}\text{F}(p,\gamma)^{18}\text{Ne}$ stellar reaction rate for temperatures greater than 0.2 GK, which is in the range of peak temperatures produced in nova explosions. Subsequent analyses of the mass $A=18$ isobars have arrived at a wide variety of results. García *et al.* calculated $E_x = 4.53$ MeV and $\Gamma = 22$ keV [12], while most recently Sherr and Fortune predicted $E_x = 4.642$ MeV and $\Gamma = 42$ keV [21]. The shell-model predictions are summarized in Table I.

Several high resolution experiments were performed to search for and measure the properties of this 3^+ state. García *et al.* studied the $^{16}\text{O}(^3\text{He},n)^{18}\text{Ne}$ reaction and reported evidence at one energy (at one angle) for a small peak which has generally been interpreted as locating the missing 3^+ state at $E_x = 4.561 \pm 0.009$ MeV [12]. This state was not seen, however, in the subsequent high-resolution (p,t) studies of Hahn *et al.* [22] and Park *et al.* [23]. Hahn *et al.* studied the $^{12}\text{C}(^{12}\text{C},^6\text{He})^{18}\text{Ne}$ and $^{20}\text{Ne}(p,t)^{18}\text{Ne}$ reactions.

TABLE I. The predicted properties of the 3^+ state from shell-model calculations are shown.

	Wiescher <i>et al.</i> [20]	García <i>et al.</i> [12]	Sherr and Fortune [21]
E_x	4.328 MeV	4.53 MeV	4.642 MeV
Γ	5 keV	22 keV	42 keV

While their resolution in the $^{12}\text{C}(^{12}\text{C}, ^6\text{He})^{18}\text{Ne}$ measurement was not sufficient to resolve the sets of states at 4.5 and at 5.1 MeV, they could separate those states in the $^{20}\text{Ne}(p,t)^{18}\text{Ne}$ measurement. They found no evidence for the existence of the 3^+ state. On the basis of the measured widths, they argued that the state previously observed in Ref. [19] at 5.09 MeV was the 2^+ state, and the state at 5.15 MeV was the 3^- . Park *et al.* also searched for the 3^+ state using the $^{20}\text{Ne}(p,t)^{18}\text{Ne}$ reaction. Using implanted ^{20}Ne targets [24], they obtained excellent energy resolution and clearly resolved the states at 4.52 and 4.59 MeV. They also found no evidence for the existence of the 3^+ state. By measuring the angular distributions from the states in the 5.1 MeV doublet, they were able to confirm the spin assignments made in Hahn *et al.* A summary of the reactions previously used to study this excitation energy region in ^{18}Ne is shown in Table II.

All of the above studies were hindered from seeing the 3^+ state by their use of reactions that suppress the population of states with unnatural parity. The $(^3\text{He},n)$ and (p,t) reactions may be regarded as the transfer of a $J=0, T=1$ particle pair. For the case of a spin zero target, such as ^{16}O or ^{20}Ne , the cross section for a direct, one-step transfer can be shown [25] to equal the square of a sum of transfer amplitudes, each characterized by the same orbital angular momentum transfer L . For a direct one-step transition in which compound nuclear processes can be neglected, the angular distribution will have a shape characteristic of L , and the state being populated must have spin and parity $J^\pi = L^{(-)^L}$. It is possible to populate states of unnatural parity by multistep processes such as $^{20}\text{Ne}(p,d)^{19}\text{Ne}(\frac{1}{2}^+)(d,t)^{18}\text{Ne}(3^+)$ [21], but such channels are typically very weak.

We studied ^{18}Ne by measuring the $^{17}\text{F}+p$ elastic scattering cross section. Since ^{17}F has a $\frac{5}{2}^+$ ground state, the ^{17}F

+ p system populates 3^+ and 2^+ states in ^{18}Ne with $l=0$ partial waves and is, therefore, very sensitive to the missing 3^+ state. By measuring the $^1\text{H}(^{17}\text{F},p)^{17}\text{F}$ excitation function, we were able to observe the interference between resonant and Rutherford scattering caused by the 3^+ state and measure its excitation energy and width [26]. From the shape of the excitation function and the angular distribution measured on resonance, the spin and parity of the state were determined.

II. THE $^1\text{H}(^{17}\text{O},p)^{17}\text{O}$ MEASUREMENT

Initially, a measurement of the $^1\text{H}(^{17}\text{O},p)^{17}\text{O}$ excitation function was made in order to test the sensitivity of scattering in inverse kinematics in our detector geometry to the properties of nuclear states. Since the ground state of ^{17}O has $J^\pi = \frac{5}{2}^+$, $^{17}\text{O}+p$ can populate 3^+ and 2^+ states in ^{18}F with $l=0$ partial waves. The energy range of the ^{17}O beam was chosen to populate the isobaric analog in ^{18}F of the 3^+ state sought in ^{18}Ne . We also included in our measurement a nearby 2^+ state in ^{18}F . This allowed us to examine the sensitivity of the resonant angular distribution to the spin and parity of the state populated.

An ^{17}O beam bombarded a $50\text{-}\mu\text{g}/\text{cm}^2$ polypropylene $(\text{CH}_2)_n$ foil. The scattered protons were detected in the Silicon Detector Array (SIDAR) [27] which was placed 19 cm from the target to cover lab angles $15^\circ \leq \theta_{\text{lab}} \leq 35^\circ$. The SIDAR is comprised of eight individual detectors each covering $\Delta\phi \approx 45^\circ$ and radial distances from 5 to 13 cm. Each detector is segmented into 16 radial 0.5-cm-wide strips. The detectors used in this experiment ranged in thickness from 100 to 500 μm . They were type YY1 detectors manufactured by Micron Semiconductor Limited [28]; the array is similar to the Louvain-Edinburgh detector array (LEDA) [29]. The SIDAR provides large solid angle coverage ($\Delta\Omega_{\text{lab}} \approx 1.1$ sr), excellent energy resolution ($\Delta E \leq 28$ keV for 5.4 MeV α particles), and high segmentation which allows for the extraction of angular distribution information while also allowing for higher total counting rates without pileup than could be obtained with a single detector of the same area. Preamplification and shaping of the detector signals were accomplished using modules designed by an Edinburgh-Rutherford Appleton Laboratory collaboration

TABLE II. List of reactions previously used to study the $E_x \approx 4.5$ MeV region of ^{18}Ne . None of these studies found conclusive evidence for the existence of a 3^+ state in ^{18}Ne .

	$^{20}\text{Ne}(p,t)^{18}\text{Ne}$	$^{16}\text{O}(^3\text{He},n)^{18}\text{Ne}$	$^{12}\text{C}(^{12}\text{C}, ^6\text{He})^{18}\text{Ne}$
Park <i>et al.</i> [23]	✓		
Hahn <i>et al.</i> [22]	✓	✓	✓
García <i>et al.</i> [12]		✓	
Nero <i>et al.</i> [19]	✓	✓	
Paddock <i>et al.</i> [14]	✓		
L'Ecuyer <i>et al.</i> [15]	✓		
Falk <i>et al.</i> [16]	✓		
Adelberger <i>et al.</i> [18]		✓	
Towle <i>et al.</i> [17]		✓	

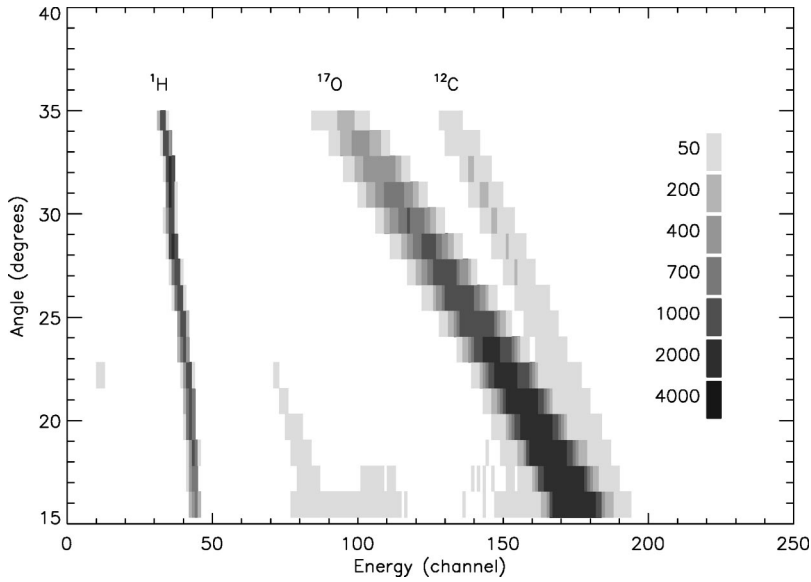


FIG. 2. A density plot showing the angle of the detected particles versus their energy. The protons from the ${}^1\text{H}({}^{17}\text{O}, p)$ reaction are cleanly separated from the ${}^{17}\text{O}$ and ${}^{12}\text{C}$ ions from the ${}^{12}\text{C}({}^{17}\text{O}, {}^{17}\text{O})$ and ${}^{12}\text{C}({}^{17}\text{O}, {}^{12}\text{C})$ reactions.

specifically for strip detector applications [30].

Proton yields were measured with the SIDAR at 19 beam energies from 9 to 13.5 MeV over a period of 4 days with ${}^{17}\text{O}$ beam currents of about 5×10^6 ${}^{17}\text{O}$ ions per second. Beam currents were intentionally kept low to simulate expected radioactive ion beam intensities. As can be seen in Fig. 2, the protons were clearly distinguishable from other scattered ions by their energy, angular dependence, and small energy spread. The yield at each energy was determined by computing the sum Y_p of the number of protons detected in all strips of the SIDAR and normalizing to the incident beam current. This normalization was achieved by monitoring the amount of ${}^{17}\text{O}$, Y_O , that was scattered from carbon in the target and detected by the SIDAR. The ${}^1\text{H}({}^{17}\text{O}, p){}^{17}\text{O}$ yield as a function of bombarding energy was calculated as

$$\sigma_{O+p} = \frac{Y_p}{Y_O E_{in} E_{out}} \times \text{const}, \quad (1)$$

where $E_{in}(E_{out})$ is the energy the beam has before (after) it transverses the target. The $E_{in}E_{out}$ factor is necessary to account for the energy dependence of the ${}^{17}\text{O}+{}^{12}\text{C}$ scattering used for beam current normalization. These normalized proton yields are plotted in Fig. 3, and the 3^+ and 2^+ resonances are clearly visible. The statistical error bars are smaller than the symbols on the plot. The measurement at 10.2 MeV was repeated at the end of the run to test the reproducibility of the system and was found to lie within the uncertainty of the measurements.

It was important that the composition of the targets be stable since the ${}^{17}\text{O}+{}^1\text{H}$ yield was being normalized to the ${}^{17}\text{O}+{}^{12}\text{C}$ scattering. Hydrogen depletion or carbon buildup on the targets could change the measured yields. The proton and total detector counting rates were monitored as a function of time to watch for changes in the target composition. The total counting rate was dominated by ${}^{17}\text{O}+{}^{12}\text{C}$ scattering at small angles. If the ratio of hydrogen to carbon atoms in the target changed, then the ratio of total to proton count-

ing rates would change. This ratio was monitored during each run, and the slope was always consistent with no change in the H/C ratio of the target. A typical plot of this is shown in Fig. 4. The fact that the measurements at 10.2 MeV were reproducible also indicates that there was no significant changes in target composition during the experiment.

A fit to the data was performed, assuming the lower-energy resonance was a 3^+ state and the higher energy resonance was a 2^+ state. The resonances were parametrized with the Breit-Wigner formalism of Blatt and Biedenharn [31] which includes the interference between the resonances and the Rutherford scattering cross section. The theoretical cross section was integrated over the angles covered by the SIDAR and averaged over the energy loss in the target. A

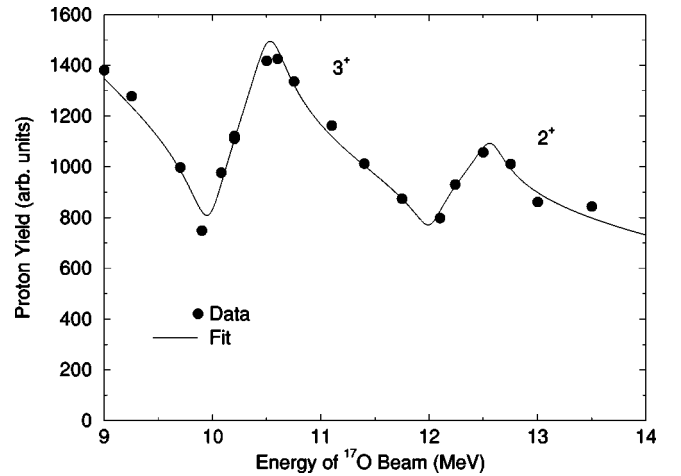


FIG. 3. The proton yields along with a five-parameter fit to the data are shown as a function of bombarding energy. The fit combines the Rutherford scattering cross section with a Breit-Wigner parametrization of the resonances and includes the interference between the two. The parameters that were allowed to vary in the fit were the normalization, the resonance energies, and the widths of the two states. The statistical error bars are smaller than the symbols on the plot.

least squares fit to the data was performed with five fit parameters: the normalization, the resonance energies of the two states, and the widths of the two states. The best fit is shown in Fig. 3, and the best-fit parameters are given in Table III along with the previously measured values [32]. The quoted uncertainties in the fit results are statistical and were determined in the standard way from the least-squares fit to the data [33]. The resonance energies (E_r) are within 3 keV of the average of the previously measured values while the widths (Γ) are within 2 keV of the previously measured values.

To test the sensitivity of the angular distribution to the spin and parity of the resonance, we ran for an extended time with a thinner ($11\text{-}\mu\text{g}/\text{cm}^2$) parylene C_8H_8 foil on both the 10.08 MeV (3^+) and 12.24 MeV (2^+) states. The use of such a thin foil was required to observe the subtle differences in angular distributions produced by the two resonances. The measured proton yields as a function of angle are shown in Fig. 5. Fits to the data were performed assuming that the resonance was a 3^+ and a 2^+ state. The differential cross section was averaged by the energy loss in the target and integrated over the solid angle covered by each strip. The only fit parameter that was allowed to vary was the normalization. A better fit ($\chi^2_\nu=1.04$) to the angular distribution at 10.08 MeV was obtained when the state was assumed to be a 3^+ state than when it was assumed to be a 2^+ state ($\chi^2_\nu=5.62$). The angular distribution at 12.24 MeV was fit much better by assuming the resonance was a 2^+ state ($\chi^2_\nu=1.09$) instead of a 3^+ state ($\chi^2_\nu=4.47$). We therefore conclude that our angular distribution measurements are indeed sensitive to the spin and parity of the state we are populating.

III. COINCIDENCE MEASUREMENTS

We had demonstrated that properties of nuclear states can be determined by measuring proton-scattering yields in inverse kinematics, but experiments with radioactive ^{17}F beams were not as straightforward for two reasons. First, the ^{17}F beam was contaminated to some extent with ^{17}O . The mass difference between the two is only one part in 6000, and it was very difficult to suppress the ^{17}O contamination in the beam. By measuring only the energy deposited in the SIDAR, it was not possible to distinguish protons scattered by ^{17}F from those scattered by ^{17}O projectiles. A second problem was that positrons from the decay of ^{17}F deposited enough energy in the 300- and 500- μm -thick detectors to

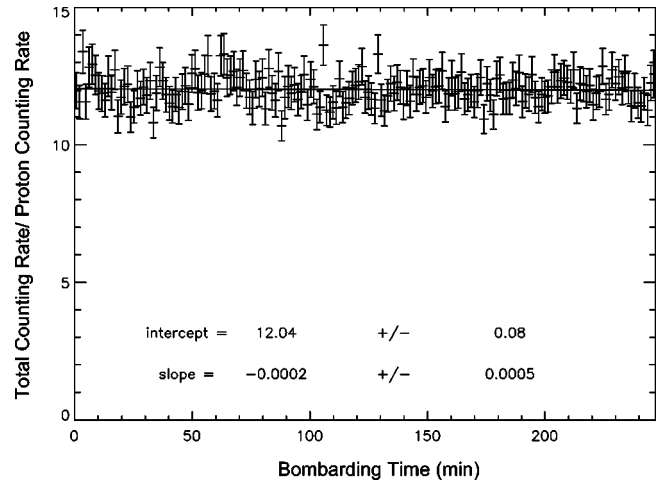


FIG. 4. The proton and total detector counting rates were measured as a function of time to monitor changes in target composition. If hydrogen-loss were occurring, then the ratio of total to proton counting rates would increase with time. A typical plot of this ratio is shown and is consistent with no hydrogen loss.

provide a significant background which overlapped the proton peak.

Both of these problems were solved by detecting the recoil ^{17}F and ^{17}O ions in coincidence with the scattered protons. An ionization counter was positioned immediately downstream of the SIDAR for this purpose. The counter was isobutane-filled and had three anodes of lengths 5, 5, and 20 cm which measured the differential energy-loss of detected ions for particle identification [34]. The entrance window was 5 cm in diameter and made from 0.9 μm Mylar which allowed for isobutane gas pressures of up to 15 Torr. The window was supported by a wire grid (3 mm spacing), and the grid wire potentials were graded to maintain uniform electric fields at the front of the detector for efficient charge collection. Field uniformity was further ensured by the use of guard rings and grading electrodes around the sensitive volume. The unscattered primary beam was prevented from entering the counter by a 1.5-cm-diameter disk placed immediately upstream of the window. The disk covered angles $\theta_{\text{lab}} \leq 2.1^\circ$, and thus for the proton angles covered by the SIDAR, the corresponding $A=17$ recoil ions ($2.6^\circ \leq \theta_{\text{lab}} \leq 3.2^\circ$) were not blocked by the disk. A drawing of the experimental configuration is shown in Fig. 6. Further details of the ionization counter are given in James *et al.* [34]. The information provided by the counter allowed the separation

TABLE III. The best-fit and previously measured resonance parameters for the two states in ^{18}F observed in the $^1\text{H}(^{17}\text{O},p)^{17}\text{O}$ measurement.

	Fit results ^a	$^{16}\text{O}(^3\text{He},p)^{18}\text{F}$ ^b	$^{17}\text{O}(p,p)^{17}\text{O}$ ^b
$J^\pi=3^+$ E_x (MeV)	6.1649 ± 0.0002	6.164 ± 0.001	6.161 ± 0.001
$J^\pi=3^+$ Γ (keV)	13.9 ± 0.2		14.0 ± 0.5
$J^\pi=2^+$ E_x (MeV)	6.2795 ± 0.0005	6.284 ± 0.001	6.281 ± 0.001
$J^\pi=2^+$ Γ (keV)	11.2 ± 0.3		10.0 ± 0.5

^aUncertainties quoted in fit results are purely statistical in nature.

^bTaken from Tilley *et al.* [32].

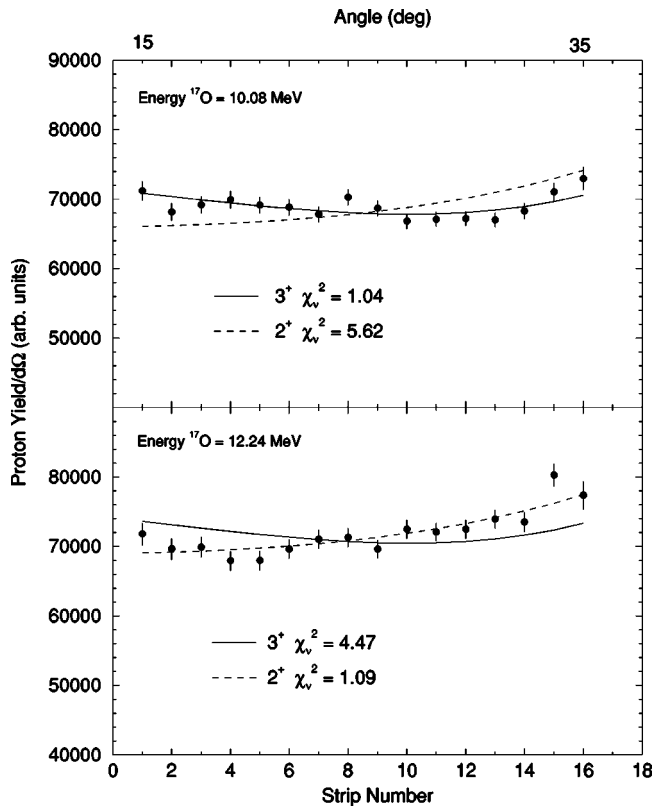


FIG. 5. The angular distributions of protons from the $^1\text{H}(^{17}\text{O},p)^{17}\text{O}$ reaction were measured at two bombarding energies. The top plot shows the angular distribution produced while running at the energy of the known 3^+ resonance. The data are better fit with an angular distribution that assumes the population of a 3^+ state. The bottom plot shows the angular distribution produced while running at the 2^+ resonance energy. In this case, the data are better fit with an angular distribution that assumes the population of a 2^+ state.

of fluorine and oxygen scattering events.

The coincidence efficiency of this new configuration was measured with the $^1\text{H}(^{17}\text{O},p)^{17}\text{O}$ reaction. An ^{17}O beam was tuned through a 4-mm aperture into the ionization counter. During the tuning procedure, the beam current was reduced by a series of upstream sieves to approximately 10^3 oxygen ions/s to prevent saturation of the counter. After the beam was satisfactorily tuned through the aperture (greater than 90% transmission), the sieves were taken out until the beam current reached 10^5 ions/s. The aperture was replaced

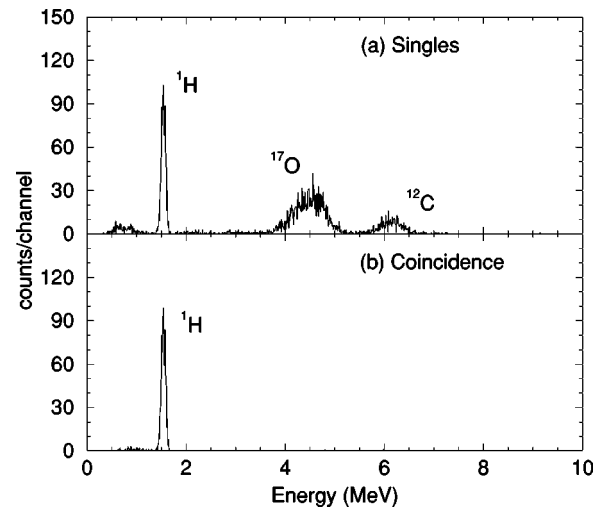


FIG. 7. (a) A particle spectrum from a ring of SIDAR strips covering lab angles $31^\circ \leq \theta_{\text{lab}} \leq 33^\circ$ is shown. A 10 MeV ^{17}O beam impinged on a $48\text{-}\mu\text{g}/\text{cm}^2$ polypropylene target. (b) Same as (a) when coincidence with recoil ^{17}O ions detected by the ionization counter was required.

by the 1.5-cm-diameter disk, and the beam was allowed to impinge on a $57\text{-}\mu\text{g}/\text{cm}^2$ polypropylene target. The effectiveness of the coincidence requirement is exhibited in Fig. 7. A particle spectrum from the SIDAR is shown without and with the coincidence requirement. When we required that there be a coincidence with an ^{17}O ion detected by the ionization counter, only the proton peak remained in the SIDAR spectrum. Coincidence efficiencies were measured at six ^{17}O beam energies between 9.25 and 13.5 MeV. The efficiency was found to be 96% and was independent of beam energy to within a few percent. This energy-independence is expected because for elastic scattering reactions the center-of-mass angles covered by the detectors only depend on the lab angles and not on the bombarding energy.

IV. THE $^1\text{H}(^{17}\text{F},p)^{17}\text{F}$ MEASUREMENTS

A. Excitation function

After the proof-of-principle measurement was performed with the ^{17}O beam, the $^1\text{H}(^{17}\text{F},p)^{17}\text{F}$ excitation function was measured. The radioactive ^{17}F beam was produced by an ISOL-type target/ion source [35] via the $^{16}\text{O}(d,n)^{17}\text{F}$ reaction using a fibrous refractory HfO_2 target bombarded with

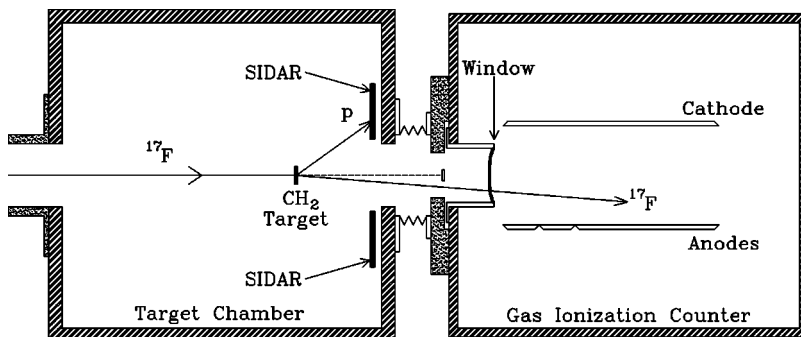


FIG. 6. The experimental configuration is shown with ^{17}F ions impinging on a polypropylene target. The scattered protons were detected in the SIDAR, while recoil ^{17}F ions were detected in coincidence in a gas-filled ionization counter. The unscattered beam was stopped by a 1.5-cm-diameter disk upstream of the ion counter.

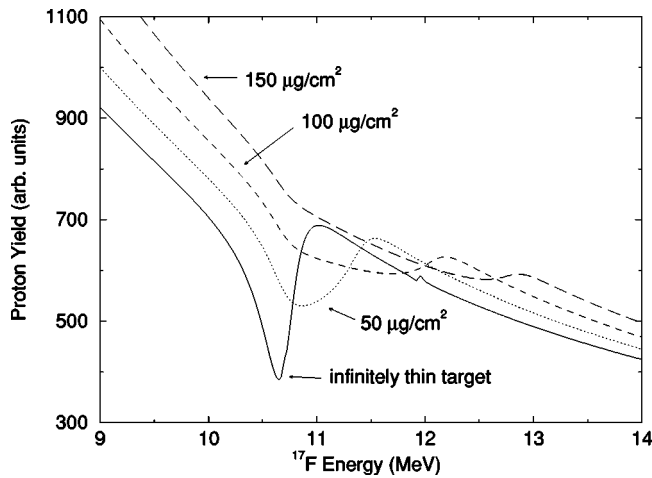


FIG. 8. The dependence of the expected excitation function on target thickness is shown. Our target thickness ($\approx 50 \mu\text{g}/\text{cm}^2$) was chosen to maximize the proton-scattering yield without washing out the resonance structure. Each curve has been normalized independently to appear on the same plot. Small contributions from the previously known states at $E_x=4.519$ and 4.590 MeV in ^{18}Ne are evident around 10.75 and 12 MeV bombarding energies in the infinitely thin target curve only.

$8 \mu\text{A}$ of 44.5 MeV deuterons from the $K=105$ Oak Ridge Isochronous Cyclotron. Aluminum vapor was fed into the target to form Al^{17}F molecules which transported the highly reactive ^{17}F atoms out of the target material and through a short (10 cm) transfer tube to an electron-beam-plasma ion source, where they were ionized and extracted [36]. After a first stage of mass analysis, the Al^{17}F^+ molecules entered a cesium charge-exchange cell where the molecules were dissociated. The resulting $^{17}\text{F}^-$ ions were then accelerated off the target/ion source high-voltage platform, analyzed by the second stage isobar separator, and then accelerated to the appropriate energy by the HRIBF tandem Van de Graaff. After passing through an energy-analyzing magnet, the ^{17}F beam was delivered to the experimental station. The average

intensity during the excitation function measurement was 8×10^3 ^{17}F ions per second on target.

The beam was tuned through a 4-mm aperture into the ionization counter where the beam purity was measured to be $^{17}\text{F}/^{17}\text{O} \approx 1000$. The transmission through the aperture after tuning was generally better than 90%. Once this tuning procedure was complete, the aperture was replaced by the 1.5-cm-diameter disk. The beam was allowed to impinge on a $48\text{-}\mu\text{g}/\text{cm}^2$ polypropylene target, and proton yields were measured. This procedure was repeated at 12 beam energies between 10 and 12 MeV. The target thickness was chosen to maximize the scattering yield without significantly degrading the resonance structure in the excitation function. The dependence of the expected excitation function on target thickness is shown in Fig. 8. Scattered protons were detected in the SIDAR which was positioned to cover angles $25^\circ \leq \theta_{\text{lab}} \leq 51^\circ$. A particle spectrum taken with the ion counter is shown in Fig. 9. Two groups are visible. The low energy group arises from ^{17}F that has scattered from hydrogen in the target. It is this group in which we are interested and that comes in coincidence with protons detected by the SIDAR. The higher energy group arises from ^{17}F that has scattered from carbon in the target. This group was used for beam current normalization.

The proton yield at each beam energy was determined using the coincidence requirement in order to avoid the troublesome subtraction of the beta-background in the thick detector spectra. This did not introduce any systematic uncertainties because the coincidence efficiency had been measured (Sec. III) to be greater than 90% and shown not to change with beam energy. The proton yields in the coincidence spectra were summed, normalized to the incident beam current, and are plotted in Fig. 10. The beam current normalization was performed using the same procedure that was used in the $^1\text{H}(^{17}\text{O},p)^{17}\text{O}$ measurement with the exception that the scattered ^{17}F ions from $^{12}\text{C}(^{17}\text{F}, ^{17}\text{F})$ detected in the ion counter were used instead of those detected in the SIDAR. There was no appreciable target degradation or

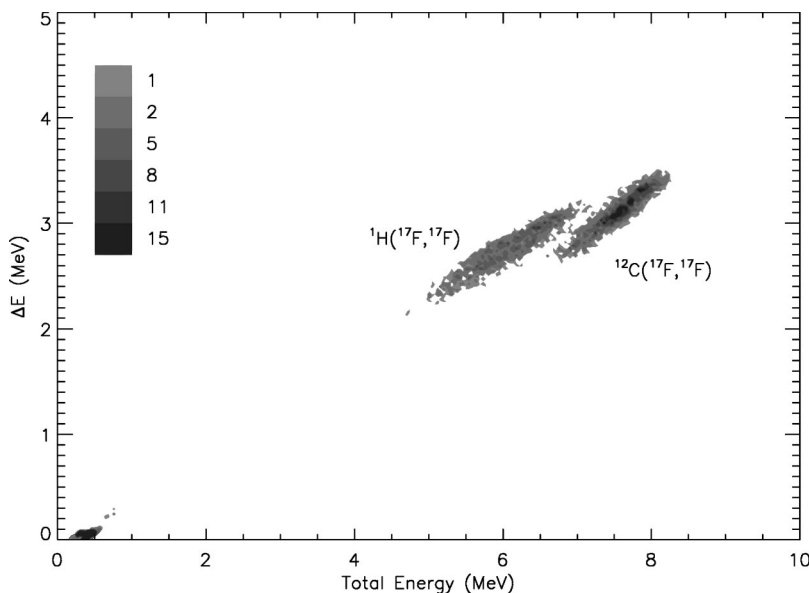


FIG. 9. A spectrum taken with the ion counter during the $^1\text{H}(^{17}\text{F}, ^{17}\text{F})$ experiment is shown. Two particle groups are visible owing to the scattering of ^{17}F from the hydrogen and carbon in the target. In this plot ΔE is the energy lost in the first anode and the total energy is the sum of energies lost in all three anodes.

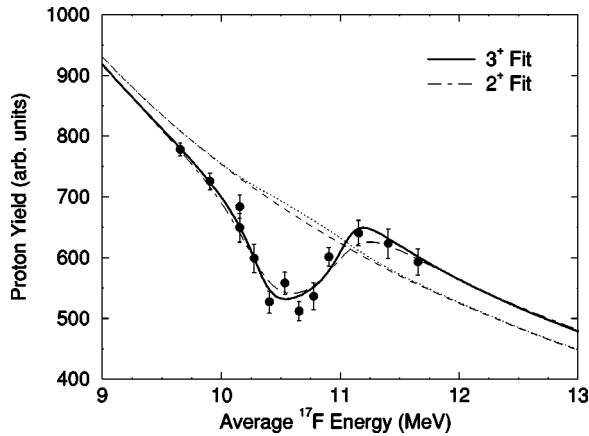


FIG. 10. The normalized proton yields are plotted as a function of the average ^{17}F beam energy in the target. The solid line is a fit to the data with three fit parameters: the normalization, the resonance energy, and the width of the 3^+ state. The dashed line shows the excitation function expected if the only resonances in this region were the previously observed 1^- and 0^+ states in ^{18}Ne . The dotted line shows the excitation function if the width of the 1^- state was 20 keV instead of the expected 0.1 keV. This curve demonstrates that the scattering anomaly could not be caused by an $l=1$ resonance. The fit assuming that the resonance is a 2^+ state is also shown.

dead-time during the experiment. The measurement at 10.15 MeV was repeated six weeks later after a break for accelerator problems to test the reproducibility of the system and found to lie within the uncertainties of the measurements. The excitation function clearly shows the presence of a resonance.

A fit to the $^1\text{H}(^{17}\text{F},p)^{17}\text{F}$ data is also shown in Fig. 10. The fit uses a Breit-Wigner parametrization of the cross section and assumes that the resonance populated has $J^\pi=3^+$. The theoretical cross section was integrated over the angles covered by the SIDAR and averaged over the energy loss in the target. The energy loss was measured with a ^{19}F beam, corrected for the mass of ^{17}F , and found to be 690 ± 50 keV, corresponding to 39 ± 3 keV in the center-of-mass system. The best fit ($\chi^2_\nu=1.19$) was obtained for a center-of-mass resonance energy of $E_r=599.8 \pm 1.5$ keV and a total resonance width of $\Gamma=18 \pm 2$ keV. Also shown in Fig. 10 is the excitation function we would expect to see if the only contributions to the yield were from Rutherford scattering and the previously observed 1^- and 0^+ states. Clearly the observed resonance is not due to a previously known state in ^{18}Ne .

B. Assignment of $J^\pi=3^+$ to the observed state

There is significant evidence that the observed resonance has $J^\pi=3^+$. The fact that the scattering anomaly is of such a shape and large amplitude indicates that the resonance must be an $l=0$ angular momentum transfer. As a demonstration of this, the excitation function we would expect to observe if the known 1^- state ($l=1$ resonance) had a width of 20 keV (instead of the expected 0.1 keV) is also shown in Fig. 10. Even with such an unphysically large width, the

contribution of an $l=1$ resonance is negligible. The resonance, therefore, is clearly due to a previously unobserved 3^+ or 2^+ state.

A fit to our data assuming that the populated state is a 2^+ resonance (also shown in Fig. 10) results in a reduced chi-square value of $\chi^2_\nu=1.72$ which is larger than the value obtained when it was assumed that the resonance had $J^\pi=3^+$ ($\chi^2_\nu=1.19$). The width required to fit the data with a 2^+ state also disagrees with the known widths of analog states in ^{18}O . The proton width can be parametrized as $\Gamma_p=C^2S\Gamma_{sp}$ where C^2 and S are the isospin Clebsch-Gordan coefficient and the single-particle spectroscopic factor, respectively [37]. Γ_{sp} denotes the partial width of a single-particle resonance located at the same energy as the resonance of interest. The quantity C^2S can be taken from the analog 3^+ state in ^{18}O as $C^2S=1.01$ [38]. The single-particle width as computed in an optical-model calculation is $\Gamma_{sp}=19$ keV [37]. If the resonance observed is indeed the analog to the 3^+ state at $E_x=5.38$ MeV in ^{18}O , then the observed width should be $\Gamma \approx \Gamma_p \approx 19$ keV. This is consistent with the observed width of 18 ± 2 keV. For comparison, the same analysis can be done for the 2^+ state at $E_x=5.26$ MeV in ^{18}O . From Li *et al.* [38], the quantity C^2S for this state is 0.35, and therefore the width one would expect for this 2^+ state would be 7 keV. The fit to our data for a 2^+ state, however, gives a width of 30 keV. This exceeds the total possible $1s_{1/2}$ single particle strength and is a factor of 4 greater than the estimated width.

In addition from inspection of the nuclear level diagram in Fig. 1, we see that there are no 2^+ states in ^{18}O in this excitation energy region for which a mirror has not already been identified in ^{18}Ne . The nucleus ^{18}O is well studied, and it is highly unlikely that there exists a 2^+ state which has never been observed at this excitation energy.

C. Measurement of the resonant angular distribution

Additional information concerning the spin and parity of the observed state can be gained by measuring the angular distribution of protons produced while bombarding at the resonance energy. This information could not simply be harvested from the existing data because sufficient statistics were not collected at any energy to allow extraction of a precise angular distribution. A new measurement of the angular distribution of scattered protons was performed using a ^{17}F beam at an energy of 11.14 MeV with a $57\text{-}\mu\text{g}/\text{cm}^2$ polypropylene target. With this beam energy and target thickness, the ^{17}F ions will be on resonance near the center of the target. Use of a thinner target would have improved the sensitivity of the measurement, but this was not practical at the beam intensities available.

In this case, beam production utilized a kinetic-ejection negative ion source [39] which has the advantage of producing negative ions directly. By avoiding the charge-exchange step of the beam-production process, somewhat higher beam currents of ^{17}F ($\sim 2 \times 10^4$ ^{17}F ions per second) could be obtained. The ^{17}O contamination of the beam, however, was much worse. Typical beam impurities were found to be $^{17}\text{O}/^{17}\text{F} \approx 15$ compared to $\approx 1/1000$ for the electron beam

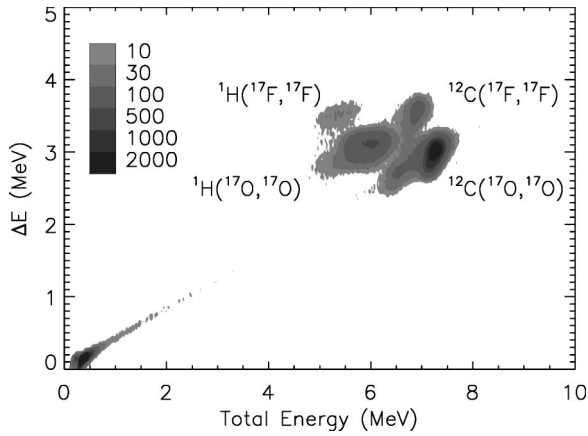


FIG. 11. A spectrum collected by the ionization counter during the measurement of the proton angular distribution is shown. A mixed ($^{17}\text{O}/^{17}\text{F} \approx 15$) beam bombarded a polypropylene target. Scattered fluorine and oxygen ions were observed in the counter. The $^1\text{H}(^{17}\text{F}, ^{17}\text{F})$ events were readily distinguished from other scattering events detected by the counter.

plasma source. Fortunately, using the coincidence-technique we were able to distinguish the $^1\text{H}(^{17}\text{F}, p)^{17}\text{F}$ events from the much more intense ^{17}O scattering background. A particle spectrum from the ionization counter is shown in Fig. 11.

The angular distribution was measured over a period of 24 hours between angles $18^\circ \leq \theta_{\text{lab}} \leq 40^\circ$ and is shown in Fig. 12. The yield at each angle was corrected for the angular dependence of the coincidence efficiency which was measured by comparing the total number of protons detected at each angle with the number of protons detected in coincidence with an ^{17}O or ^{17}F ion. Also shown is a fit ($\chi^2_\nu = 1.14$) to the data assuming that the populated resonance has $J^\pi = 3^+$ and a width $\Gamma = 18$ keV. The only parameter

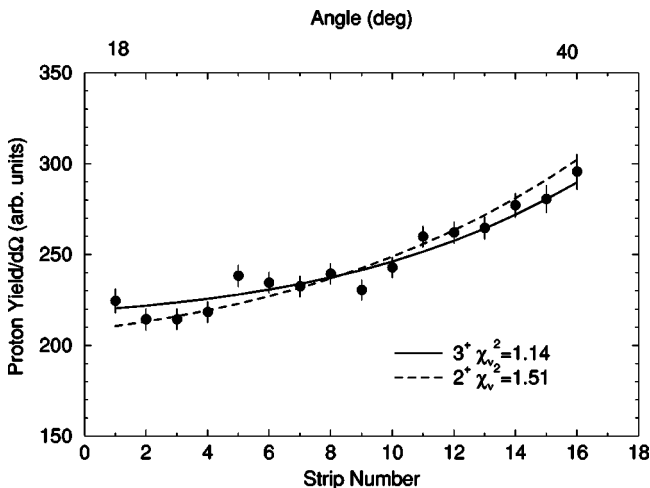


FIG. 12. The angular distribution of protons produced on resonance is shown. The solid line is a fit assuming the resonance has $(J^\pi, \Gamma) = (3^+, 18 \text{ keV})$ and varying only the normalization as a fit parameter. The dashed line assumes $(J^\pi, \Gamma) = (2^+, 19 \text{ keV})$; 19 keV was used because that is the maximum single particle width of a 2^+ resonance at this energy. The data are slightly better fit by a 3^+ assignment.

that was allowed to vary was the normalization. In addition, a fit was performed assuming that the resonance has $J^\pi = 2^+$ and the maximum single particle width of 19 keV. The fit in this case was not as good ($\chi^2_\nu = 1.51$) and is also shown in Fig. 12.

We therefore conclude that the observed resonance is the long-sought 3^+ state in ^{18}Ne for the following reasons. The shape and amplitude of the scattering anomaly rule out all but a $J^\pi = 3^+$ or 2^+ assignment. The observed excitation function and angular distribution are better fit by a 3^+ assignment. The properties of the observed resonance (E_x, Γ) are consistent with the expectations from mirror symmetry for a 3^+ assignment, while they are not consistent with the assumption of 2^+ . There are, furthermore, no 2^+ states available in ^{18}O for which this state could be the isospin mirror.

D. Systematic uncertainties of the results

An obvious source of systematic uncertainty is the beam energy calibration. The HRIBF energy-analyzing magnet was originally calibrated using a time-of-flight technique [40]. This calibration was checked with a precision of $\Delta E_{\text{c.m.}} = \pm 0.2$ keV by measuring the $^1\text{H}(^{19}\text{F}, \alpha)^{16}\text{O}$ excitation function in the region of the ^{20}Ne resonance at $E_{\text{c.m.}} = 828$ keV [41]. It should be noted that while the proton resonance energy of this state is listed correctly as 872.11 keV in Table 20.29 of Tilley *et al.* [41], the excitation energy listed in Table 20.29 (and the master table) does not reflect the currently accepted mass of ^{20}Ne . The excitation energy of this state, listed as 13676 ± 3 keV, should instead be 13672.0 ± 0.3 keV [42]. A ^{19}F beam was used to bombard a $48\text{-}\mu\text{g}/\text{cm}^2$ CH_2 target, and alpha-particle yields were measured in the SIDAR for six beam energies between 16.3 and 16.8 MeV. The beam current normalization was performed by measuring the number of carbon atoms scattered from the target into the SIDAR and then correcting this by the E^{-2} dependence of the Rutherford scattering cross section. The number of alpha particles detected was summed over all strips and then normalized by the carbon yield. This normalized alpha-particle yield is plotted in Fig. 13 along with a two-parameter fit to the data. The fitting function was the equation for the thick-target yield given in Rolfs and Rodney [43] as

$$Y(E) = A \left[\arctan\left(\frac{E - E_r}{\Gamma/2}\right) - \arctan\left(\frac{E - E_r - \Delta}{\Gamma/2}\right) \right], \quad (2)$$

where A is a normalization constant, Δ is the energy loss in the target which was measured to be 690 keV, and Γ is the width of the state which is known to be 4.5 keV [41]. The normalization and the resonance energy were allowed to vary in the fit. The best fit was obtained for a resonance energy of 828.0 ± 0.2 keV; this agrees with the known value of 828.2 ± 0.2 keV. This uncertainty in the fit results in a negligible uncertainty in the center-of-mass energy of 0.2 keV.

Another source of systematic uncertainty may arise from the required coincidence with the ion counter. To investigate possible systematic effects related to this coincidence requirement, the proton yields were extracted from the singles

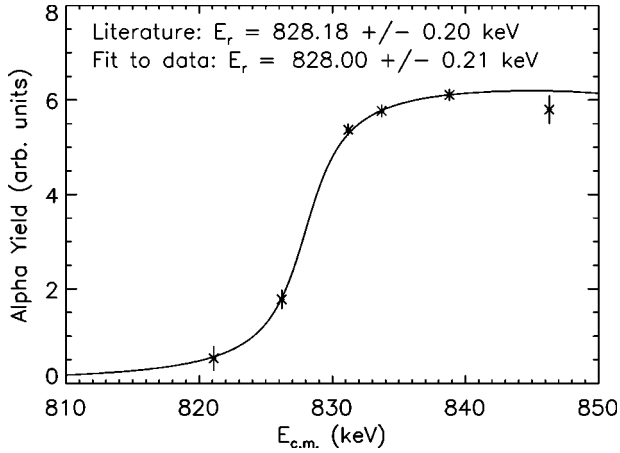


FIG. 13. In order to check the beam energy calibration, the $^1\text{H}(^{19}\text{F}, \alpha)^{16}\text{O}$ excitation function was measured in the region of the ^{20}Ne resonance at $E_{\text{c.m.}} = 828$ keV. A fit to the data was performed with the resonance energy and normalization as fit parameters. The best fit was obtained for a resonance energy of 828.0 ± 0.2 keV which is within the uncertainty of the accepted value [41].

data set, instead of the spectra gated on a ^{17}F coincidence. In some of the detectors, the tail of the beta peak overlapped with the protons, and therefore use of the singles data would require background subtraction from the proton peak. Only in the four thinnest (100- μm -thick) detectors was the background small enough to allow this subtraction. Since only four out of the eight detectors were of the 100 μm variety, the proton yields extracted from the singles spectra only have one-half of the number of events contained in the coincidence excitation function, and therefore the uncertainty in the yield at each energy is larger. Also during the first three proton yield measurements (10, 10.25, and 10.5 MeV), no thin detectors were used. The excitation function extracted from the singles data is shown in Fig. 14. The resonance energy and width that resulted in the best fit ($\chi^2_{\nu} = 0.41$) differed by no more than 2 keV from those obtained from the coincidence data excitation function.

To further understand other systematic uncertainties of our measurement, the dependence of the best-fit results on

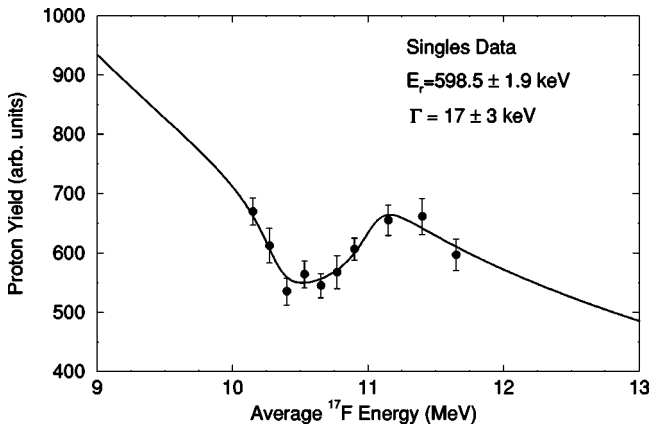


FIG. 14. The $^1\text{H}(^{17}\text{F}, p)^{17}\text{F}$ excitation function extracted from the singles data is shown. The best-fit resonance energy and width differ by ≤ 2 keV from those extracted from the coincidence data.

TABLE IV. The dependence of the best-fit parameters is shown as a function of the target energy-loss used in the fitting routine.

Target ΔE	χ^2_{ν}	E_r (keV)	Γ (keV)
640 keV	1.02	600.6 ± 1.3	17 ± 2
690 keV	1.19	599.8 ± 1.5	18 ± 2
740 keV	1.34	598.7 ± 1.5	18 ± 2

different parameters was investigated. Since we measured the energy loss to be 690 ± 50 keV, we recalculated the best-fit parameters using energy losses of 640 and 740 keV. The results are given in Table IV. The best-fit results changed by less than 2 keV as the assumed energy-loss was changed.

In addition, an R -matrix fit to the coincidence data was performed instead of the Breit-Wigner fit. The R -matrix code MULTI [44] was used, and the best fit ($\chi^2_{\nu} = 1.43$) was obtained for a resonance energy of 600.9 ± 1.2 keV and a width of 17.2 ± 1.2 keV.

All of the above recalculations of the best-fit parameters resulted in variations in the resonance energy of less than 2 keV and in the width of no more than 1 keV. From this and from the previous study of the $^1\text{H}(^{17}\text{O}, p)^{17}\text{O}$ excitation function, we estimate the systematic uncertainty for the resonance energy to be 2 keV and for the width to be 1 keV. We, therefore, adopt values of $E_r = 599.8 \pm 1.5_{\text{stat}} \pm 2.0_{\text{sys}}$ keV and $\Gamma = 18 \pm 2_{\text{stat}} \pm 1_{\text{sys}}$ keV for the resonance energy and width of the 3^+ state.

E. ^{18}Ne excitation energy of the 3^+ state

The corresponding excitation energy in ^{18}Ne was calculated by combining this resonance energy with the tabulated mass excesses

$$E_x = Q + E_r = \Delta(^1\text{H}) + \Delta(^{17}\text{F}) - \Delta(^{18}\text{Ne}) + E_r. \quad (3)$$

The mass excesses of ^1H and ^{17}F are known [45] to be 7288.969 ± 0.001 keV and 1951.701 ± 0.248 keV, respectively. The mass excess of ^{18}Ne (5316.8 ± 1.5 keV) was taken from the measurement of Magnus *et al.* [46] that was incorrectly quoted in the 1997 mass compilation [45]. Combining these masses yields an excitation energy of the 3^+ state in ^{18}Ne of 4523.7 ± 2.9 keV which is within the range spanned by predictions [12,20,21]. This is also very close to the known 1^- state in ^{18}Ne at 4.519 MeV and explains why the 3^+ state was not previously observed in reactions which strongly populate natural-parity states. A nuclear level diagram showing our measured excitation energy for the 3^+ state is shown in Fig. 15.

V. THE $^{17}\text{F}(p, \gamma)^{18}\text{Ne}$ RATE

The astrophysical $^{17}\text{F}(p, \gamma)^{18}\text{Ne}$ rate is made up of contributions from ^{18}Ne resonances and direct capture. The direct-capture cross section was calculated by García *et al.* [12] using the formalism of Rolfs [47], and the resulting reaction rate is unchanged from Ref. [48].

Only the first three resonances above the $^{17}\text{F} + p$ threshold

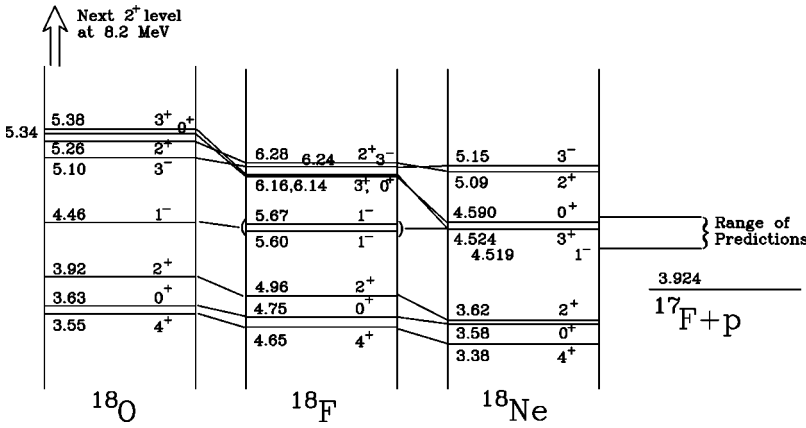


FIG. 15. The $A=18$ isobars are shown with the addition of the newly observed 3^+ state. The excitation energy is within the range spanned by the predictions at 4523.7 ± 2.9 keV.

are low enough in energy to significantly contribute to the $^{17}\text{F}(p, \gamma)^{18}\text{Ne}$ stellar reaction rate for $T \leq 2$ GK. The contributions of the resonances were calculated from the resonance properties in Table V. The properties of the 1^- and 0^+ states as well as the γ partial width of the 3^+ state are taken from García *et al.* The uncertainties in the resonance energies for the 1^- and 0^+ state are smaller than reported by García *et al.* because of the improved measurement of the ^{18}Ne mass excess [46]. The γ partial widths were estimated in García *et al.* by assuming that the ^{18}Ne decays have the same reduced transition strengths as the analogous transitions in ^{18}O . The 1^- and 0^+ resonances are narrow, and therefore their contributions to the $^{17}\text{F}(p, \gamma)^{18}\text{Ne}$ reaction rate can be calculated as [13]

$$N_A \langle \sigma v \rangle_{1^-} = \frac{630.0}{(T_9)^{3/2}} \exp\left(-11.605 \times \frac{0.595}{T_9}\right) \text{cm}^3 \text{mole}^{-1} \text{s}^{-1},$$

$$N_A \langle \sigma v \rangle_{0^+} = \frac{13.99}{(T_9)^{3/2}} \exp\left(-11.605 \times \frac{0.666}{T_9}\right) \text{cm}^3 \text{mole}^{-1} \text{s}^{-1}. \quad (4)$$

Because of the large width of the 3^+ resonance, its contribution to the $^{17}\text{F}(p, \gamma)^{18}\text{Ne}$ reaction rate must be calculated by numerically integrating the S factor and scaling the widths by the Coulomb penetrability [48]. The 3^+ component of the reaction rate is shown in Fig. 16 in comparison with the rates from the previous predictions of the 3^+ resonance parameters [12,20,21]. Because the resonance energy of the 3^+ state is 37 keV lower than was found by García *et al.*, its contribution to the $^{17}\text{F}(p, \gamma)^{18}\text{Ne}$ reaction rate is a factor of ~ 2 larger at $T = 0.5$ GK than the prediction of Bardayan and Smith [48]. It is different, however, by up to 2

orders of magnitude from the prediction of Wiescher *et al.* and up to 1 order of magnitude from the prediction of Sherr and Fortune.

The resonant as well as the direct capture contributions to the $^{17}\text{F}(p, \gamma)^{18}\text{Ne}$ stellar rate are displayed in Fig. 17. The total rate which is the sum of these four components is also displayed in Fig. 17 and tabulated as a function of temperature in Table VI. The 3^+ resonance dominates the reaction rate at temperatures greater than 0.5 GK while the rate is dominated by direct capture for lower temperatures. The uncertainties in the rate are also given in Table VI. The greatest uncertainty in the rate at high temperatures is due to the uncertainty in the γ partial width of the 3^+ state. At low temperatures the uncertainty is dominated by the uncertainty in the direct capture amplitude. The present uncertainty in the rate, which varies from 15 to 40% over the temperature range, is much smaller than the orders of magnitude uncertainty that previously existed due to the unknown excitation energy of the 3^+ state.

The stellar temperatures and densities for which the $^{17}\text{F}(p, \gamma)^{18}\text{Ne}$ rate is faster than the ^{17}F β -decay rate are shown in Fig. 18. A hydrogen mass fraction of $X_H = 0.365$ [49] for the initial composition of the accreted matter was assumed. Peak temperatures and densities of typical nova explosions are also shown on the plot. Most of the peak conditions result in the $^{17}\text{F}(p, \gamma)^{18}\text{Ne}$ rate being faster than the ^{17}F β -decay rate. The effect that the improved calculation of the $^{17}\text{F}(p, \gamma)^{18}\text{Ne}$ rate has on the abundances produced in nova models is currently being investigated [50].

Expressions for the relevant nuclear reaction rates as analytic functions of the stellar temperature are crucial input for models of complex astrophysical events such as novae. We present analytic expressions for the $^{17}\text{F}(p, \gamma)^{18}\text{Ne}$ rate in two popular formats: the first is similar to that used in the Caugh-

TABLE V. The properties of the resonances used in the calculation of the $^{17}\text{F}(p, \gamma)^{18}\text{Ne}$ rate are shown.

	1^-	3^+	0^+
E_r (keV)	595 ± 5	600 ± 2	666 ± 5
Γ_p (keV)	0.1^a	18 ± 2	1.0^a
Γ_γ (keV)	$(1.5 \pm 0.3) \times 10^{-5}$	$(2.5 \pm 1.6) \times 10^{-5}$	$(1.0 \pm 0.2) \times 10^{-6}$

^aProton widths from Ref. [12]. Uncertainties in the proton widths are not quoted because $\Gamma_p \gg \Gamma_\gamma$, and therefore an uncertainty in the proton width introduces a negligible uncertainty in the reaction rate.

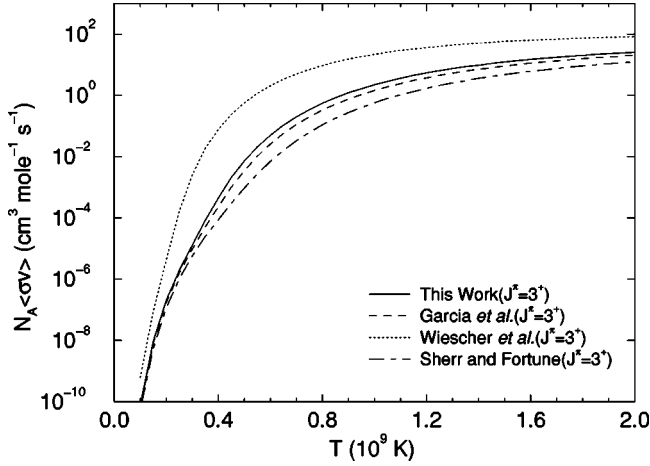


FIG. 16. The contribution to the $^{17}\text{F}(p, \gamma)^{18}\text{Ne}$ reaction rate from the 3^+ state is plotted as a function of stellar temperature. This is compared to estimates of the rate from previously published predictions of the resonance parameters from García *et al.* [12], Wiescher *et al.* [20], and Sherr and Fortune [21]. Determining the resonance energy of the 3^+ state has cleared up an uncertainty in its contribution which spanned orders of magnitude.

lan and Fowler reaction rate compilation [51], and the second is similar to expressions in Thielemann *et al.* [52]. The total reaction rate was fitted over the temperature range $0.1 \text{ GK} \leq T \leq 2.0 \text{ GK}$. The residuals of the fit are less than 20% for the Caughlan and Fowler format and less than 0.6% for the Thielemann format. The rate expressions using parameters resulting from the fits are given in Table VII. Further details of the fitting procedure can be found in Ref. [48].

VI. CONCLUSIONS

Knowledge of the $^{17}\text{F}(p, \gamma)^{18}\text{Ne}$ reaction rate is crucial for understanding stellar events such as novae and x-ray bursts. Before these measurements, the rate was uncertain by

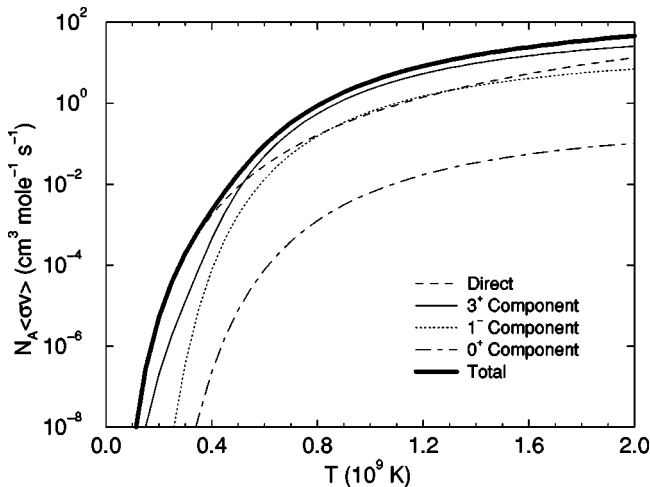


FIG. 17. The contributions from the resonances to the $^{17}\text{F}(p, \gamma)^{18}\text{Ne}$ rate are shown along with the direct-capture rate. The total rate is the sum of these components. The 3^+ resonance dominates the rate at temperatures above 0.5 GK, while below that temperature, the rate is dominated by direct capture.

TABLE VI. The $^{17}\text{F}(p, \gamma)^{18}\text{Ne}$ rate is shown as a function of stellar temperature.

$T(10^9 \text{ K})$	$N_A \langle \sigma v \rangle (\text{cm}^3 \text{ mole}^{-1} \text{ s}^{-1})$
0.1	$(2.68 \pm 0.38) \times 10^{-9}$
0.2	$(5.15 \pm 0.75) \times 10^{-6}$
0.3	$(1.97 \pm 0.29) \times 10^{-4}$
0.4	$(2.29 \pm 0.40) \times 10^{-3}$
0.5	$(1.77 \pm 0.49) \times 10^{-2}$
0.6	$(9.29 \pm 3.28) \times 10^{-2}$
0.7	$(3.32 \pm 1.30) \times 10^{-1}$
0.8	$(8.80 \pm 3.61) \times 10^{-1}$
0.9	$(1.88 \pm 0.78) \times 10^0$
1.0	$(3.43 \pm 1.44) \times 10^0$
1.5	$(1.97 \pm 0.78) \times 10^1$
2.0	$(4.62 \pm 1.64) \times 10^1$

orders of magnitudes (e.g., Refs. [12,20,21]) depending on the excitation energy of an expected but never conclusively observed 3^+ state in ^{18}Ne . By measuring the $^1\text{H}(^{17}\text{F}, p)^{17}\text{F}$ excitation function at the HRIBF, we have observed the previously missing 3^+ state and determined its properties, $E_r = 599.8 \pm 1.5_{\text{stat}} \pm 2.0_{\text{sys}}$ keV ($E_x = 4523.7 \pm 2.9$ keV) and $\Gamma = 18 \pm 2_{\text{stat}} \pm 1_{\text{sys}}$ keV. The 3^+ state dominates the reaction rate at temperatures above 0.5 GK and is, therefore, very important for x-ray bursts. At temperatures below this, such as in novae, direct capture dominates the rate.

While we have resolved the greatest uncertainty in the $^{17}\text{F}(p, \gamma)^{18}\text{Ne}$ rate, other uncertainties still exist. At high temperatures, the greatest uncertainty in the rate arises from the unmeasured γ partial width of the 3^+ state. At low temperatures, the uncertainty is dominated by the unmeasured direct capture contribution to the rate. Both of these could be addressed with a measurement of the $^{17}\text{F}(p, \gamma)^{18}\text{Ne}$ cross section. Work is underway to make this measurement at the

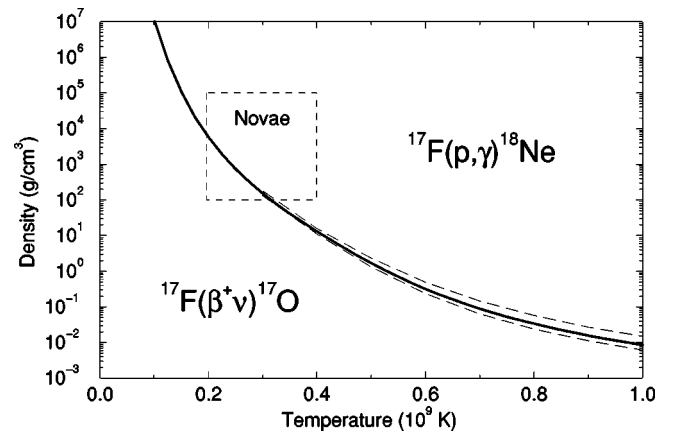


FIG. 18. The plotted line shows the temperature-density conditions for which the $^{17}\text{F}(p, \gamma)^{18}\text{Ne}$ rate is equal to the ^{17}F β -decay rate. Above the line, the $^{17}\text{F}(p, \gamma)^{18}\text{Ne}$ rate dominates the destruction of ^{17}F . Conditions characteristic of nova explosions are also shown. The long-dashed lines show the variation in the boundary owing to the uncertainties (quoted in Table VI) in the $^{17}\text{F}(p, \gamma)^{18}\text{Ne}$ rate.

TABLE VII. Fit results and reaction rate expressions for the $^{17}\text{F}(p, \gamma)^{18}\text{Ne}$ rate.

Analytic form	$N_A \langle \sigma v \rangle$ ($\text{cm}^3 \text{ mole}^{-1} \text{ s}^{-1}$)
Caughlan and Fowler [51]	$4.81 \times 10^7 T_9^{-2/3} \exp(-18.0 T_9^{-1/3}) (1 + 2.31 \times 10^{-2} T_9^{1/3} - 2.32 \times 10^{-1} T_9^{2/3} - 4.40 \times 10^{-2} T_9 + 4.26 \times 10^{-2} T_9^{4/3} + 1.54 \times 10^{-2} T_9^{5/3}) + 2.36 \times 10^3 T_9^{-3/2} \exp(-6.96/T_9) + 6.300 \times 10^2 T_9^{-3/2} \exp(-6.92/T_9) + 1.399 \times 10^1 T_9^{-3/2} \exp(-7.72/T_9)$
Thielemann <i>et al.</i> [52]	$\exp(2.6357 \times 10^1 + 6.7829 \times 10^{-2} T_9^{-1} - 2.0195 \times 10^1 T_9^{-1/3} - 1.0068 \times 10^1 T_9^{1/3} + 4.7875 \times 10^0 T_9 - 1.1482 \times 10^0 T_9^{5/3} - 4.1554 \times 10^{-1} \ln T_9) + \exp(3.2659 \times 10^1 - 9.1645 \times 10^{-1} T_9^{-1} - 1.5977 \times 10^2 T_9^{-1/3} + 1.2833 \times 10^2 T_9^{1/3} + 2.6893 \times 10^0 T_9 - 2.0447 \times 10^0 T_9^{5/3} - 9.0961 \times 10^1 \ln T_9)$

HRIBF [53] using the Daresbury Recoil Separator [34] but must wait on the development of ^{17}F beams of higher intensity.

ACKNOWLEDGMENTS

We thank the staff of the HRIBF whose hard work made these experiments possible. Oak Ridge National Laboratory

is managed by UT-Battelle, LLC, for the U.S. Department of Energy under Contract No. DE-AC05-00OR22725. The Joint Institute for Heavy Ion Research has as member institutions the University of Tennessee, Vanderbilt University, and the Oak Ridge National Laboratory; it is supported by the members and by the Department of Energy. The work was supported in part by the U.S. DOE under Contract No. DE-FG02-91ER-40609.

-
- [1] R. P. Kraft, *Astrophys. J.* **139**, 457 (1964).
[2] S. Starrfield, *Phys. Rep.* **311**, 371 (1999).
[3] S. A. Glasner, E. Livne, and J. W. Truran, *Astrophys. J.* **475**, 754 (1997).
[4] Y. Chin, C. Henkel, N. Langer, and R. Mauersberger, *Astrophys. J. Lett.* **512**, L143 (1999).
[5] S. N. Shore, G. Sonneborn, S. Starrfield, and R. Gonzalez-Riestra, *Astrophys. J.* **421**, 344 (1994).
[6] J. Gómez-Gomar, M. Hernanz, J. José, and J. Isern, *Mon. Not. R. Astron. Soc.* **296**, 913 (1998).
[7] M. J. Harris, J. E. Naya, B. J. Teegarden, T. L. Cline, N. Gehrels, D. M. Palmer, R. Ramaty, and H. Seifert, *Astrophys. J.* **522**, 424 (1999).
[8] R. E. Taam, S. E. Woosley, T. A. Weaver, and D. Q. Lamb, *Astrophys. J.* **413**, 324 (1993).
[9] M. Wiescher, H. Schatz, and A. E. Champagne, *Philos. Trans. R. Soc. London, Ser. A* **356**, 2105 (1998).
[10] M. Wiescher, J. Görres, and H. Schatz, *J. Phys. G* **25**, R133 (1999).
[11] H. Schatz *et al.*, *Phys. Rep.* **294**, 167 (1998).
[12] A. García, E. G. Adelberger, P. V. Magnus, D. M. Markoff, K. B. Swartz, M. S. Smith, K. I. Hahn, N. Bateman, and P. D. Parker, *Phys. Rev. C* **43**, 2012 (1991).
[13] D. D. Clayton, *Principles of Stellar Evolution and Nucleosynthesis* (Cambridge University Press, Cambridge, 1983).
[14] R. A. Paddock, *Phys. Rev. C* **5**, 485 (1972).
[15] J. L'Ecuyer, R. D. Gill, K. Ramavataram, N. S. Chant, and D. G. Montague, *Phys. Rev. C* **2**, 116 (1970).
[16] W. R. Falk, R. J. Kidney, P. Kulisic, and G. K. Tandon, *Nucl. Phys.* **A157**, 241 (1970).
[17] J. H. Towle and G. J. Wall, *Nucl. Phys.* **A118**, 500 (1968).
[18] E. G. Adelberger and A. B. McDonald, *Nucl. Phys.* **A145**, 497 (1970).
[19] A. V. Nero, E. G. Adelberger, and F. S. Dietrich, *Phys. Rev. C* **24**, 1864 (1981).
[20] M. Wiescher, J. Görres, and F.-K. Thielemann, *Astrophys. J.* **326**, 384 (1988).
[21] R. Sherr and H. T. Fortune, *Phys. Rev. C* **58**, 3292 (1998).
[22] K. I. Hahn *et al.*, *Phys. Rev. C* **54**, 1999 (1996).
[23] S. H. Park *et al.*, *Phys. Rev. C* **59**, 1182 (1999).
[24] M. S. Smith, P. V. Magnus, K. I. Hahn, A. J. Howard, P. D. Parker, A. E. Champagne, and Z. Q. Mao, *Nucl. Phys.* **A536**, 333 (1992).
[25] N. K. Glendenning, *Phys. Rev.* **137**, 102 (1965).
[26] D. W. Bardayan *et al.*, *Phys. Rev. Lett.* **83**, 45 (1999).
[27] D. W. Bardayan, Ph.D. thesis, Yale University, 1999.
[28] Micron Semiconductor Ltd., Lancing, Sussex BN15 8UN, England.
[29] T. Davinson *et al.*, *Nucl. Instrum. Methods Phys. Res. A* (in press).
[30] S. L. Thomas, T. Davinson, and A. C. Shotton, *Nucl. Instrum. Methods Phys. Res. A* **288**, 212 (1990).
[31] J. M. Blatt and L. C. Biedenharn, *Rev. Mod. Phys.* **24**, 258 (1952).
[32] D. R. Tilley, H. R. Weller, C. M. Cheves, and R. M. Chasteler, *Nucl. Phys.* **A595**, 1 (1995).
[33] P. R. Bevington, *Data Reduction and Error Analysis for the Physical Sciences* (McGraw-Hill, New York, 1969).
[34] A. N. James, T. P. Morrison, K. L. Ying, K. A. Connell, H. G. Price, and J. Simpson, *Nucl. Instrum. Methods Phys. Res. A* **267**, 144 (1988).

- [35] G. D. Alton and J. R. Beene, *J. Phys. G* **24**, 1347 (1998).
- [36] R. F. Welton, R. L. Auble, J. R. Beene, J. C. Blackmon, J. Kormicki, P. E. Mueller, D. W. Stracener, and C. L. Williams, *Nucl. Instrum. Methods Phys. Res. B* **159**, 116 (1999).
- [37] C. Iliadis, *Nucl. Phys.* **A618**, 166 (1997).
- [38] T. K. Li, D. Dehnhard, Ronald E. Brown, and P. J. Ellis, *Phys. Rev. C* **13**, 55 (1976).
- [39] G. D. Alton, Y. Liu, C. Williams, and S. N. Murray, in *Heavy Ion Accelerator Technology: Eighth International Conference, 1999*, edited by K. W. Shepard, AIP Conf. Proc. No. 473 (American Institute of Physics, Woodbury, 1999), p. 330.
- [40] D. K. Olsen *et al.*, *Nucl. Instrum. Methods Phys. Res. A* **254**, 1 (1987).
- [41] D. R. Tilley, C. M. Cheves, J. H. Kelley, S. Raman, and H. R. Weller, *Nucl. Phys.* **A636**, 247 (1998).
- [42] D. R. Tilley (private communication).
- [43] C. E. Rolfs and W. S. Rodney, *Cauldrons in the Cosmos* (University of Chicago Press, Chicago, 1988).
- [44] R. O. Nelson, E. G. Bilpuch, and G. E. Mitchell, *Nucl. Instrum. Methods Phys. Res. A* **236**, 128 (1985).
- [45] G. Audi, O. Bersillon, J. Blachot, and A. H. Wapstra, *Nucl. Phys.* **A624**, 1 (1997).
- [46] P. V. Magnus, E. G. Adelberger, and A. García, *Phys. Rev. C* **49**, 1755 (1994).
- [47] C. Rolfs, *Nucl. Phys.* **A217**, 29 (1973).
- [48] D. W. Bardayan and M. S. Smith, *Phys. Rev. C* **56**, 1647 (1997).
- [49] M. Politano, S. Starrfield, J. W. Truran, A. Weiss, and W. M. Sparks, *Astrophys. J.* **448**, 807 (1995).
- [50] M. S. Smith *et al.* (unpublished).
- [51] G. R. Caughlan and W. A. Fowler, *At. Data Nucl. Data Tables* **40**, 283 (1988).
- [52] F.-K. Thielemann, M. Arnould, and J. Truran, in *Advances in Nuclear Astrophysics, 1987*, edited by E. Vangioni-Flam, J. Audouze, M. Casse, J.-P. Chieze, and J. Tran Thanh Van (Editions Frontieres, Gif-sur-Yvette, 1987).
- [53] M. S. Smith *et al.*, in *Stellar Evolution, Stellar Explosions and Galactic Chemical Evolution, Oak Ridge, 1997*, edited by A. Mezzacappa (Institute of Physics, Bristol, 1998), p. 511.